Magneto-optical spectroscopy with arbitrarily polarized intensity-modulated light in ⁴He atoms

He Wang ●, Teng Wu ●, Haidong Wang ●, Xiang Peng ●,* and Hong Guo ●†

State Key Laboratory of Advanced Optical Communication Systems and Networks, Department of Electronics,
and Center for Quantum Information Technology, Peking University, Beijing 100871, China

We present both a theoretical and experimental study of the magneto-optical spectra induced with intensity-modulated resonant laser light that synchronously pumps and detects the metastable ⁴He atoms in the presence of a quasistatic magnetic field. We extend previous work and derive complete analytical expressions for the resonance signals by taking into account arbitrary magnetic-field directions and arbitrary light polarizations. The analytical results are derived by solving the Liouville equation using the irreducible tensor formalism on the assumption of low light power. We discuss the potential application of the derived analytical results in constructing and optimizing a dead-zone-free all-optical atomic magnetometer.

I. INTRODUCTION

Magneto-optical spectroscopy of spin-polarized atomic vapors is a powerful tool and forms the basis for a variety of atomic sensors. One of the most prominent applications is atomic magnetometry. Atomic magnetometry, or optical magnetometry, is one of the most sensitive methods for measuring magnetic fields [1,2] and has found a wide range of applications in magnetoencephalography [3], magnetic particle imaging [4], mapping the geomagnetic field [5], space exploration [6], nuclear magnetic resonance [7], and fundamental physics [8]. Optical magnetometers use resonant light interacting with atomic vapors (usually helium or an alkali metal) in the presence of a quasistatic magnetic field. A comprehensive overview of various optical magnetometers has been given in Ref. [9]. The intensity and polarization of the light transmitted through the atomic vapor are modified by the precessing macroscopic atomic magnetic moments under the influence of a bias magnetic field. By detecting the intensity or polarization of the transmitted light, one obtains the Larmor precession frequency ω_0, which is proportional to the strength of the external magnetic field.

A common type of optical magnetometers is the magnetically driven optical magnetometer, in which a precessing macroscopic atomic magnetic moment is driven by a radio-frequency (rf) magnetic field. The full spectra of magnetically driven optical magnetometers with circularly or linearly polarized light have been studied in Refs. [10–13] and a generalized theory with arbitrarily polarized light has been investigated in Refs. [14,15]. Magnetically silent (also all-optical) atomic magnetometers which are based on optically driven precession have been realized in a Bell-Bloom configuration [16,17] and some extended configurations combining the nonlinear magneto-optical rotation technique [18,19]. This type of magnetometer, using modulated light field to replace the rf magnetic field, avoids the crosstalk effect between adjacent magnetometers [20]. The spectra of all-optical atomic magnetometers with polarization-modulated light have been investigated in Refs. [21,22]. The spectra of intensity-modulated [23] or frequency-modulated [24] schemes have only been analyzed with circularly or linearly polarized light when the magnetic-field direction is taken into account.

The full spectra of optical magnetometers, which contain all information about the resonance signals, play a vital role in practical applications. For instance, the orientational dependence of the optically detected resonance signal amplitude is used to determine the dead-zone effect. The dead zone, where the signal is too small to be detected when the magnetic field is oriented in a certain direction, is a feature inherent to the optical magnetometer [21]. Based on the spectra of optical magnetometers, various techniques have been developed to avoid the dead zones. In magnetically driven optical magnetometers, the dead-zone effect is eliminated by employing multiple cells [14], controlling the polarization of the linearly polarized light and the direction of the rf magnetic field [25,26]. In all-optical atomic magnetometers, a dead-zone-free atomic magnetometer is realized by adding signals from two separated orthogonally polarized beams [27,28], using multiple beams to realize a triple-resonance scheme [29], controlling the polarization of the linearly polarized light in an intensity-modulated magnetometer [30], modulating the light polarization between linear and circular polarization [21] or between two orthogonal linear polarizations [22].

In this paper we study the magneto-optical spectra produced by all-optical atomic magnetometers with intensity-modulated resonant laser light. Two independent groups of magnetic resonance signals at the fundamental and the second harmonic of the Larmor frequency are obtained. We derive complete analytical expressions for the resonance signals. Previous work on such resonance signals [23,24,31] was limited to a specific polarized light or magnetic-field direction. The results presented here are more general because they are valid for arbitrary light polarizations and for arbitrary magnetic-field directions. We also present experimental

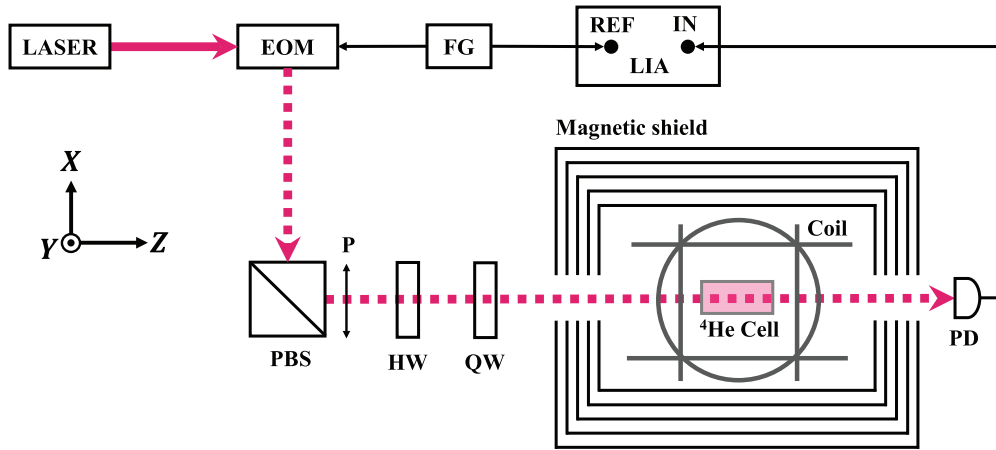*xiangpeng@pku.edu.cn
†hongguo@pku.edu.cn

FIG. 1. Schematic of the experimental setup. A set of three-dimensional coils produces an arbitrarily oriented magnetic field $\boldsymbol{B}$. The metastable ^{4}He atoms exposed to the external magnetic field $\boldsymbol{B}$ are enclosed in a glass cell, inside a five-layer μ-metal magnetic shield. Resonant polarized light, propagating along the Z axis, is used for optical pumping and probing. The fast axis of the quarter waveplate (QW) is fixed along the X axis. A polarization beam splitter (PBS) and a half waveplate (HW) prepare linearly polarized light of adjustable orientation α with respect to the X axis. The ellipticity of the light polarization is determined by α. An electro-optical modulator (EOM) is used to modulate the light intensity and is driven with a function generator (FG). A lock-in amplifier (LIA), whose reference signal (REF) comes from the FG, is used to extract the amplitude and the phase of the signal from the photodiode (PD).

results of the resonance signals, which show agreement with analytical expressions derived from the developed theoretical model. The restriction of the theoretical model is also discussed in this paper. In addition, a dead-zone-free all-optical magnetometer could be designed utilizing the derived dependence of the signal amplitude on light polarization and magnetic-field direction.

The paper is organized as follows. In Sec. II we introduce the experimental setup. In Sec. III the theoretical model is described and the analytical expressions of the full spectra are derived. In Sec. IV we compare the theoretical predictions with preliminary experimental results and discuss the applications of the expressions. Section V contains a summary and the conclusions.

II. EXPERIMENTAL SETUP

The experimental setup is illustrated in Fig. 1, which is in a Bell-Bloom configuration. The central part of the magnetometer is a 50-cm-diam, 70-cm-long cylindrical glass atomic vapor cell (at room temperature, 0.4 Torr), which is placed inside a five-layer μ-metal magnetic shield. A 35-MHz radio-frequency discharge is used to produce metastable ^{4}He atoms. A resonant polarized light, derived from a distributed feedback fiber laser module (Koheras ADJUSTIK Y10), is used for optical pumping and probing. The laser frequency is stabilized to the ^{4}He D_0 transition line ($2\,^3S_1$–$2\,^3P_0$) using a polarization spectroscopy system [32]. The light power is 1.5 mW, which is under the low-light-power approximation because the light power is in the range where the resonance signal amplitude grows quadratically with the light power [31]. The intensity of the light is sinusoidally modulated at frequency ω with an electro-optical modulator. An arbitrarily oriented static magnetic field $\boldsymbol{B}$ of about 5000 nT is generated by a set of three-dimensional coils. A lock-in amplifier (Zurich Instruments, Model No. HF2LI) is used to extract the

amplitude and the phase of the signal from the photodiode detecting the transmitted power of the light.

The Jones vector of the fully polarized light can be defined as $[\cos\epsilon - i\sin\epsilon\ 0]^{\mathrm{T}}$, where ϵ is the ellipticity of the light polarization [14]. After the half waveplate, the angle between the linear polarization and the X axis is α. Thus the angle α is equal to the ellipticity ϵ. The polarization of the light is along the X axis when α is $0°$, while the polarization is along the negative direction of the Y axis when α is $90°$.

III. THEORETICAL MODEL

The magnetic-field coordinate system and the light-field coordinate system are shown in Fig. 2(a). The direction of the external magnetic field $\boldsymbol{B}$ is typically chosen as the z axis. The propagation direction of the light beam is chosen as the Z axis. Here ϕ and θ relate the two coordinate systems; ϕ is the angle between the light propagation direction and the
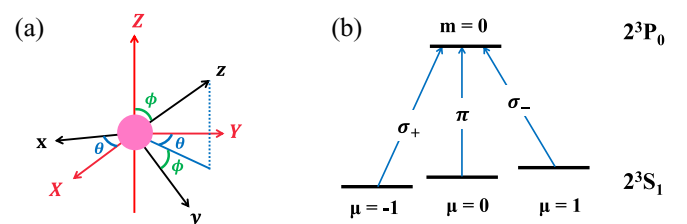

FIG. 2. (a) Lowercase x, y, and z form the magnetic-field coordinate system (black lines) and the capital X, Y, and Z denote the light-field coordinate system (red or gray lines). Here ϕ is the angle between the Z and z axes and θ is the angle between the Y axis and the projection of the z axis on the X-Y plane. (b) Magnetic sublevels of $2\,^3S_1$ and $2\,^3P_0$ in ^{4}He, with $\sigma_\pm$- and π-polarized components of a polarized light field with the quantization axis along the magnetic field $\boldsymbol{B}$. Here $\mu = 1, 0, -1$ are the $2\,^3S_1$ metastable sublevel indices and $m = 0$ is the $2\,^3P_0$ magnetic sublevel index.

external magnetic field and θ is the angle between the Y axis and the projection of the z axis on the X-Y plane. In this paper, calculations are made in the magnetic-field coordinates, in which the quantization axis is along the magnetic field $\boldsymbol{B}$. We set $\hbar = 1$ throughout the text.

For ^{4}He atoms with nuclear spin $I = 0$, the magnetic sublevels of the $2\,^3S_1$ state with angular momentum $J_\mu = 1$ and the $2\,^3P_0$ state with angular momentum $J_m = 0$ are shown in Fig. 2(b). The metastable- and excited-state Zeeman sublevels are labeled μ and m, respectively.

At low light power, i.e., when the pumping rate is much smaller than the relaxation rate, the optical pumping and probing by a single laser beam can be described by a three-step process (pumping, precession, and probing) [18]. In the first step, orientation and alignment moments in the ^{4}He metastable state are created due to absorption of the pumping light. In the second step, these moments undergo Larmor precession in the magnetic field. The intensity and polarization of the light transmitted through the atomic vapor are modified by the precessing moments. In the third step, this modification can be detected by measuring the absorption of the same pumping light transmitted through the atomic medium. The time evolution of the metastable-state density matrix ρ is described by the Liouville equation [33]

$$\frac{d\rho}{dt} = -i[\mathcal{H}, \rho] + \rho_{\text{pump}} - \rho_{\text{relax}}, \quad (1)$$

where $\mathcal{H} = \mathcal{H}_0 + \mathcal{H}_M$, $\mathcal{H}_0$ is the unperturbed Hamiltonian, $\mathcal{H}_M$ is the magnetic-field–atom interaction Hamiltonian, ρ_{pump} is a source term produced by optical pumping, and ρ_{relax} describes the relaxation processes.

The theoretical model related to the metastable state of ^{4}He atoms is formulated in terms of the spin-1 spherical basis. The irreducible spherical tensor operators have the commutation relations [34]

$$[\mathsf{J}_z, \mathsf{T}_q^{(\kappa)}] = q\mathsf{T}_q^{(\kappa)}, \quad (2a)$$

$$[\mathsf{J}_\pm, \mathsf{T}_q^{(\kappa)}] = \sqrt{\kappa(\kappa+1) - q(q \pm 1)}\,\mathsf{T}_{q\pm1}^{(\kappa)}, \quad (2b)$$

where $\mathsf{J}_\pm = \mathsf{J}_x \pm i\mathsf{J}_y$, $\kappa = 0, 1, 2$ is the rank of irreducible tensors, and $q = -\kappa, -\kappa + 1, \ldots, \kappa - 1, \kappa$ are the components. The density matrix ρ of the three metastable sublevels can be decomposed in the basis of irreducible spherical tensor operators

$$\rho = \frac{\mathsf{I}}{3} + \sum_{\kappa=1}^{2} \sum_{q=-\kappa}^{\kappa} (-1)^q \langle \mathsf{T}_{-q}^{(\kappa)} \rangle \mathsf{T}_q^{(\kappa)}, \quad (3)$$

where I is the identity operator and the rank-1 portions satisfy $\mathsf{T}_0^{(1)} = \mathsf{J}_z/\sqrt{2}$, $\mathsf{T}_{-1}^{(1)} = \mathsf{J}_-/2$, and $\mathsf{T}_1^{(1)} = -\mathsf{J}_+/2$. The angular brackets denote the average values of the operators and $\langle \mathsf{T}_q^{(\kappa)} \rangle = \text{Tr}[\rho \mathsf{T}_q^{(\kappa)}]$. The three vector moments $\langle \mathsf{J}_z \rangle$, $\langle \mathsf{J}_+ \rangle$, and $\langle \mathsf{J}_- \rangle$ represent the orientation of the medium, while the five second-rank tensor components $\langle \mathsf{T}_q^{(2)} \rangle$, $q = -2, -1, 0, 1, 2$, represent its alignment.

A. Step 1: Creation of atomic multipole moments by optical pumping

A weak monochromatic laser light with complex polarization vector $\mathbf{e}$, resonant with the ^{4}He D_0 transition line, is used

for optical pumping. The influence of ^{4}He D_1 and D_2 transition lines can be ignored because the D_0 line is completely resolved. The metastable state of ^{4}He atoms can be split into three Zeeman sublevels, while the excited state do not split. The atoms in the three Zeeman sublevels of the metastable state are optically excited into the $2\,^3P_0$ level by a polarized light according to the selection rule. The excited $2\,^3P_0$ state atoms spontaneously decay back to the $2\,^3S_0$ sublevels with equal probability. Thus the polarized light establishes the polarization of the metastable ^{4}He atoms. This process in which atomic polarization produced in the metastable state is due to certain metastable-state sublevels absorbing light more strongly than others is called the depopulation pumping process [33].

The light-atom interaction of the depopulation pumping process can be represented by the effective Hamiltonian operator $\mathcal{H}_{\text{eff}}$ whose elements are [33]

$$\langle \mu | \mathcal{H}_{\text{eff}} | \mu' \rangle = \frac{E_0^2}{\Gamma_e} \sum_m \langle \mu | \mathbf{e}^* \cdot \mathbf{D} | m \rangle \langle m | \mathbf{e} \cdot \mathbf{D} | \mu' \rangle L(\Delta), \quad (4)$$

where E_0 and $\mathbf{e}$ are the electric-field amplitude and the Jones vector of the pump light, respectively, the asterisk denotes the complex conjugate, $\mathbf{D}$ is the electric dipole operator, Γ_e is the spontaneous decay rate of the excited state, $L(\Delta) = \Gamma_e/(\Delta + i\Gamma_e)$, and Δ is the detuning of the laser frequency from the D_0 transition line. In the magnetic-field coordinate system, the Jones vector of the pumping light can be written as

$$\mathbf{e} = \begin{bmatrix} e_x \\ e_y \\ e_z \end{bmatrix} = \begin{bmatrix} \cos\epsilon\cos\theta + i\sin\epsilon\sin\theta \\ \cos\epsilon\sin\theta\cos\phi - i\sin\epsilon\cos\theta\cos\phi \\ \cos\epsilon\sin\theta\sin\phi - i\sin\epsilon\cos\theta\sin\phi \end{bmatrix},$$

which can be expanded as $\mathbf{e} = e^{-1}\hat{e}_{-1} + e^0\hat{e}_0 + e^1\hat{e}_1$ in the spherical basis, where the covariant spherical basis unit vectors are $\hat{e}_0 = \hat{z}$ and $\hat{e}_{\pm1} = \mp\frac{1}{\sqrt{2}}(\hat{x} \pm i\hat{y})$, and the contravariant spherical components of the spherical basis unit vectors are connected to the Cartesian components according to $e^{\pm1} = \mp\frac{1}{\sqrt{2}}(e_x \mp ie_y)$ and $e^0 = e_z$. For the ^{4}He D_0 transition line, the matrix elements $\langle m|\mathbf{D}|\mu \rangle$ of the dipole operator (which can be found in Ref. [35])

$$\langle m|\mathbf{D}|\mu \rangle = -\frac{D_0}{\sqrt{3}}[\hat{e}_1 \quad \hat{e}_0 \quad \hat{e}_{-1}], \quad (5)$$

where $D_0 = 2.5312 q_e a_0$, q_e is the electron charge, and a_0 is the Bohr radius. The columns are ordered according to decreasing magnetic quantum numbers. Then one obtains

$$\sum_m \mathbf{e}^* \cdot \mathbf{D} |m\rangle\langle m| \mathbf{e} \cdot \mathbf{D} = \frac{D_0^2}{3}\Phi, \quad (6)$$

where

$$\Phi = \begin{pmatrix} |e^{-1}|^2 & -e^{-1*}e^0 & e^{-1*}e^1 \\ -e^{0*}e^{-1} & |e^0|^2 & -e^{0*}e^1 \\ e^{1*}e^{-1} & -e^{1*}e^0 & |e^1|^2 \end{pmatrix}. \quad (7)$$

Notice that Φ is Hermitian and satisfies $\text{Tr}[\Phi] = 1$. Then one obtains

$$\mathcal{H}_{\text{eff}} = \frac{E_0^2 D_0^2}{3\Gamma_e}\Phi L(\Delta). \quad (8)$$

The electric dipole transitions couple only to vector moments and second-rank tensor moments [34] and Φ can also be expanded as irreducible tensors

$$\Phi = \frac{\mathsf{I}}{3} + \sum_{\kappa=1}^{2} \sum_{q=-\kappa}^{\kappa} (-1)^q \langle \mathsf{T}_{-q}^{(\kappa)} \rangle_L \mathsf{T}_q^{(\kappa)}, \qquad (9)$$

where $\langle \mathsf{T}_q^{(\kappa)} \rangle_L = \text{Tr}[\Phi \mathsf{T}_q^{(\kappa)}]$; detailed expressions are given by Eqs. (A1).

The effective Hamiltonian operator $\mathcal{H}_{\text{eff}}$ can be written also in terms of a Hermitian light-shift operator $\delta\varepsilon$ and a Hermitian light-absorption operator $\delta\Gamma$ [33],

$$\mathcal{H}_{\text{eff}} = \delta\varepsilon - i\delta\Gamma/2. \qquad (10)$$

Thus, the light-absorption operator $\delta\Gamma$ is proportional to Φ. The produced polarization due to depopulation pumping is proportional to the absorption of the pumping light [33]. For convenience, we introduce the polarization vector $\boldsymbol{v}_L$,

$$\boldsymbol{v}_L \equiv \left[\langle \mathsf{J}_+ \rangle_L \langle \mathsf{J}_z \rangle_L \langle \mathsf{J}_- \rangle_L \langle \mathsf{T}_2^{(2)} \rangle_L \langle \mathsf{T}_1^{(2)} \rangle_L \langle \mathsf{T}_0^{(2)} \rangle_L \langle \mathsf{T}_{-1}^{(2)} \rangle_L \langle \mathsf{T}_{-2}^{(2)} \rangle_L \right]^{\text{T}}, \qquad (11)$$

and the state vector $\boldsymbol{v}$,

$$\boldsymbol{v} \equiv \left[\langle \mathsf{J}_+ \rangle \langle \mathsf{J}_z \rangle \langle \mathsf{J}_- \rangle \langle \mathsf{T}_2^{(2)} \rangle \langle \mathsf{T}_1^{(2)} \rangle \langle \mathsf{T}_0^{(2)} \rangle \langle \mathsf{T}_{-1}^{(2)} \rangle \langle \mathsf{T}_{-2}^{(2)} \rangle \right]^{\text{T}}. \qquad (12)$$

Then the contribution of the polarized light to the state vector $\boldsymbol{v}$ due to depopulation pumping can be written as

$$\left(\frac{d\boldsymbol{v}}{dt} \right)_L = \gamma_{\text{op}} \boldsymbol{v}_L, \qquad (13)$$

where γ_{op} is the pumping rate. The modulation of the light intensity yields a modulation of the pumping rate $\gamma_{\text{op}} = \gamma_p(1 + \Omega \cos \omega t)$, where γ_p is a time-independent pumping constant [23] and Ω is the depth of modulation ($0 \leqslant \Omega \leqslant 1$). The light field is supposed to be weak so that the light broadening can be neglected.

Furthermore, the frequency-modulated light, where the frequency of the pumping light is modulated closer and further from resonance, yielding a modulation on the spectral line shape $L(\Delta)$, can also be used to produce a contribution similar to Eq. (13). The polarization-modulated light would yield a modulation on the matrix Φ and induce magnetic resonance transitions when the Larmor frequency is an integer multiple of the modulation frequency [36].

Generally, the light-atom interaction transfers the light polarization to the atomic polarization. The modulation of the light parameters yields a modulation on the light-atom interaction. Accompanied by the evolution of the macroscopic atomic magnetic moments in the bias magnetic field and the relaxation processes, the modulation of the light-atom interaction produces a magnetic resonance signal.

B. Step 2: Evolution of atomic multipole moments

Since the direction of the external magnetic field is chosen as the quantization axis, the interaction Hamiltonian $\mathcal{H}_M$ between the atom and the magnetic field can be written as

$$\mathcal{H}_M = -\boldsymbol{\mu} \cdot \boldsymbol{B} = -\omega_0 \mathsf{J}_z, \qquad (14)$$

where $\boldsymbol{\mu}$ is the magnetic moment, $\boldsymbol{\mu} = \gamma \mathbf{J}$, $\omega_0 = \gamma B$, γ is the free-electron gyromagnetic ratio of the metastable state $2\,^3S_1$ of ^{4}He, and $\gamma/2\pi \approx 28.025$ Hz/nT. Substituting Eqs. (2), (3), and (14) into Eq. (1) gives

$$\left(\frac{d\langle \mathsf{T}_q^{(\kappa)} \rangle}{dt} \right)_M = -i\omega_0 q \langle \mathsf{T}_q^{(\kappa)} \rangle. \qquad (15)$$

With Eq. (12), one can rewrite Eq. (15) as a matrix equation

$$\left(\frac{d\boldsymbol{v}}{dt} \right)_M = -i\mathbb{O}\boldsymbol{v}, \qquad (16)$$

where the matrix $\mathbb{O}$ is

$$\mathbb{O} = \begin{pmatrix} \omega_0 & 0 & 0 & 0 & 0 & 0 & 0 & 0 \\ 0 & 0 & 0 & 0 & 0 & 0 & 0 & 0 \\ 0 & 0 & -\omega_0 & 0 & 0 & 0 & 0 & 0 \\ 0 & 0 & 0 & 2\omega_0 & 0 & 0 & 0 & 0 \\ 0 & 0 & 0 & 0 & \omega_0 & 0 & 0 & 0 \\ 0 & 0 & 0 & 0 & 0 & 0 & 0 & 0 \\ 0 & 0 & 0 & 0 & 0 & 0 & -\omega_0 & 0 \\ 0 & 0 & 0 & 0 & 0 & 0 & 0 & -2\omega_0 \end{pmatrix}. \qquad (17)$$

Here we assume that the eight components decay with a single relaxation rate Γ, which can produce particularly simple and elegant expressions [34]. Then the effect of polarization relaxation can be written as

$$\left(\frac{d\boldsymbol{v}}{dt} \right)_R = -\Gamma\boldsymbol{v}. \qquad (18)$$

C. Steady-state solution

The total equation can be written as

$$\frac{d\boldsymbol{v}}{dt} = -i\mathbb{O}\boldsymbol{v} + \gamma_{\text{op}}\boldsymbol{v}_L - \Gamma\boldsymbol{v}. \qquad (19)$$

The equation is similar to the Bloch equations with the main difference being that the dynamics of both the three orientation components and the five alignment components are taken into account [11]. The analytical solutions of Eq. (19) can be obtained and we only take into account the steady-state solution, which is Eq. (A2).

D. Step 3: Optically detection

The modulation of the light intensity yields a modulation of the probing rate. Thus the intensity of transmitted light is proportional to the quantity L_A [23],

$$L_A = g(1 + \Omega \cos \omega t)\text{Tr}[\rho\Phi], \qquad (20)$$

where g is the saturation parameter defined as $g \equiv \gamma_p/\Gamma$. Substituting Eqs. (3), (9), (A1), and (A2) into Eq. (20), one obtains

$$L_A = g^2 \Omega(1 + \Omega \cos \omega t)(P_{\text{IN}} \cos \omega t + P_{\text{QU}} \sin \omega t), \qquad (21)$$

where

$$P_{\text{IN}} = f_1(\theta, \phi, \epsilon)[A_1(\omega_0) + A_1(-\omega_0)]$$
$$+ f_2(\theta, \phi, \epsilon)[A_2(2\omega_0) + A_2(-2\omega_0)], \quad (22a)$$

$$P_{\text{QU}} = f_1(\theta, \phi, \epsilon)[D_1(\omega_0) + D_1(-\omega_0)]$$
$$+ f_2(\theta, \phi, \epsilon)[D_2(2\omega_0) + D_2(-2\omega_0)], \quad (22b)$$

with resonance line shapes

$$A_1(\omega_0) = \frac{\Gamma^2}{(\omega - \omega_0)^2 + \Gamma^2}, \quad (23a)$$

$$A_2(2\omega_0) = \frac{\Gamma^2}{(\omega - 2\omega_0)^2 + \Gamma^2}, \quad (23b)$$

$$D_1(\omega_0) = \frac{\Gamma(\omega - \omega_0)}{(\omega - \omega_0)^2 + \Gamma^2}, \quad (23c)$$

$$D_2(2\omega_0) = \frac{\Gamma(\omega - 2\omega_0)}{(\omega - 2\omega_0)^2 + \Gamma^2} \quad (23d)$$

and $f_1(\theta, \phi, \epsilon)$ and $f_2(\theta, \phi, \epsilon)$ shown in the Appendix [see Eqs. (A3)]. Note that in the quantity L_A there are other line shapes related to the Hanle effect and these line shapes are ignored because the modulation frequency and the Larmor frequency are much larger than the relaxation rate, i.e., $\omega, \omega_0 \gg \Gamma$ [31].

From Eqs. (22) we can conclude that the phase and the linewidth of the signal are independent of the magnetic-field direction and the ellipticity of the light polarization. Applying the rotating-wave approximation, the terms $A_1(-\omega_0)$, $A_2(-2\omega_0)$, $D_1(-\omega_0)$, and $D_2(-2\omega_0)$ can be neglected to simplify the expressions.

E. Validity of the theoretical model

We note that these solutions are valid only at low light power, i.e., $\gamma_{\text{op}} \ll \Gamma$, which indicates that the lifetime of the metastable-state polarization is much less than one optical pumping cycle [31]. This low-light-power restriction guarantees that the steady-state conditions are reached in steps 1 and 2. The Hanle resonance centered at $\omega_0 = 0$ is also ignored because $\omega_0 \gg \Gamma$ as we discussed above. In addition, for atoms with angular momenta $F > 1$, the atomic multipole moments with order $\kappa > 2$ must be ignored when applying the theoretical model. The production of higher-order ($\kappa > 2$) multipole moments and their transfer back to $\kappa = 1, 2$ moments limit the validity of the theoretical model [10].

IV. EXPERIMENTAL RESULTS AND DISCUSSION

From Eqs. (22) we know that the amplitudes of the signals demodulated at the modulation frequency ω are proportional to the modulation depth Ω, while the signals demodulated at twice the modulation frequency 2ω are proportional to Ω^2. The signals at both the fundamental and the second harmonic of the modulation frequency have the same dependence on the magnetic-field direction and the ellipticity of the light polarization. Figure 3 shows the amplitude and phase signals demodulated by a lock-in amplifier at frequency $2\omega_0$. The peak-to-peak frequency deviation of the phase signal
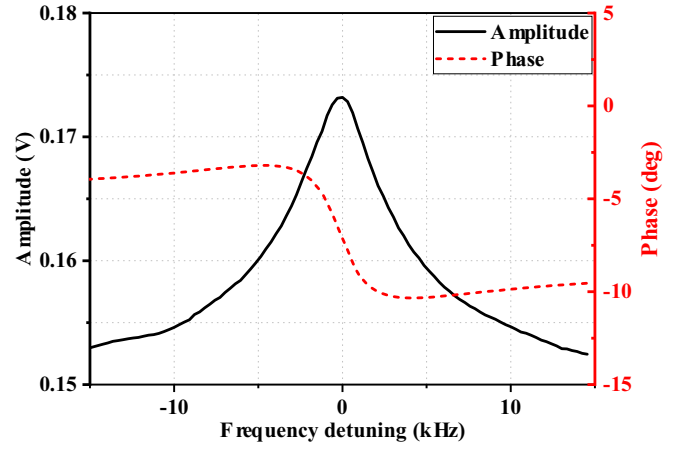

FIG. 3. Amplitude (solid black line) and phase (dashed red line) signals demodulated by a lock-in amplifier at reference frequency $2\omega_0$ as a function of the frequency detuning $\omega/2 - \omega_0$.

(linewidth) is about 6 kHz, which is broadened by factors, e.g., radio-frequency discharge and magnetic-field gradient.

First, we consider two special cases: One is the circularly polarized light $\epsilon = \pm\frac{\pi}{4}$, for which we get

$$f_1\left(\theta, \phi, \pm\frac{\pi}{4}\right) = \frac{1}{4}\sin^2\phi(\cos^2\phi + 1), \quad (24a)$$

$$f_2\left(\theta, \phi, \pm\frac{\pi}{4}\right) = \frac{\sin^4\phi}{16}, \quad (24b)$$

and the other is the linearly polarized light $\epsilon = 0$, for which we obtain

$$f_1(\theta, \phi, 0) = \sin^2\theta \sin^2\phi(1 - \sin^2\theta \sin^2\phi), \quad (25a)$$

$$f_2(\theta, \phi, 0) = \tfrac{1}{4}(1 - \sin^2\theta \sin^2\phi)^2. \quad (25b)$$

These analytical expressions of the two special cases are equivalent to the theoretical predictions from Ref. [23]. We know that there are dead zones in the cases of both circularly and linearly polarized light. A dead-zone-free all-optical magnetometer is realized by exploiting the angular information in the observed resonance signals induced with the linearly polarized light [30].

To verify general cases, the experiments with arbitrarily polarized light in an arbitrarily oriented external magnetic field are performed. From Eqs. (22) and Fig. 4 one obtains the dependence of the resonance signal amplitudes on the external magnetic-field direction and the ellipticity of the light polarization. Here the angle α is set in the range of $0°$–$90°$. Figure 4 indicates that the experimental results show agreement with our theoretical predications. The error bar is the standard error of multiple readings. The readings are made by scanning the resonance signal for several times after the half waveplate is fixed. The unapparent standard errors show the consistency of different scans and thus the stability of the light power. The residual deviations between the experimental results and the theoretical predictions indicate that there are still other error sources, such as the manual rotations of the half waveplate and the imperfections of optical components. The *in situ* method to measure and control the light polarization (within the vapor cell) [37] might be useful for controlling the systematic errors
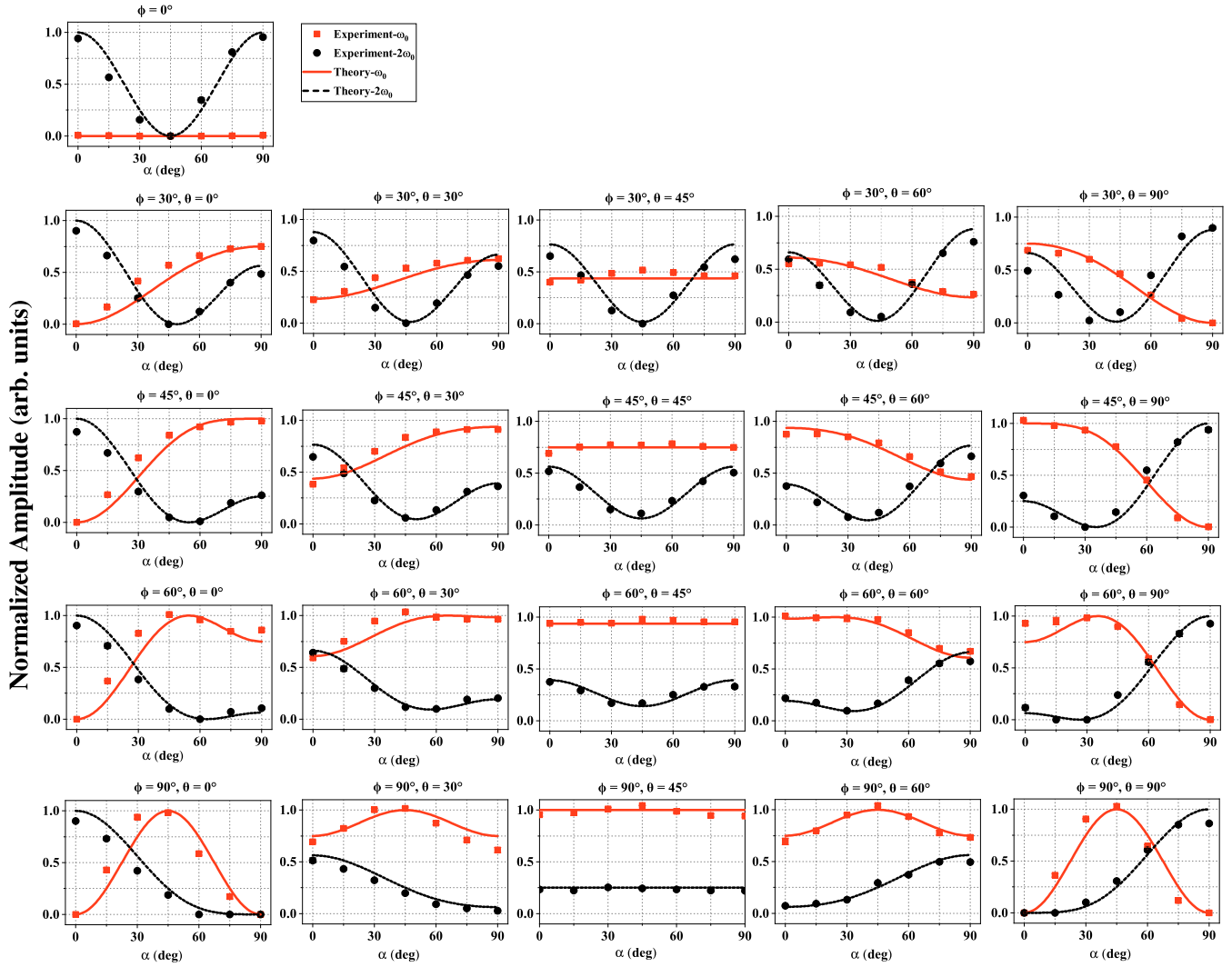
FIG. 4. Experimental (dots) and theoretical (line) results for the normalized amplitudes (proportional to f_1 and f_2) of ω_0 (solid red lines) and $2\omega_0$ (dashed black lines) resonances versus the ellipticity of the light polarization. For each plot, the magnetic-field direction which is defined with ϕ and θ [see the definitions in Fig. 2(a)] is different. The error bar shows the standard error of multiple readings, which is on the same scale as the symbol size. Since θ has no effect on the signal amplitude when the light propagates along the magnetic field **B** ($\phi = 0°$), only one plot is given.

caused by the mischaracterization of the light polarization due to the atomic vapor cell walls or other optical elements.

We can draw some useful conclusions from Fig. 4. First, whatever the ellipticity of the light polarization is, the amplitude of the resonance signal at ω_0 always vanishes when the light propagates along the magnetic field (see the $\phi = 0°$ plot). Second, the amplitude of the resonance signal at ω_0 is independent of α when θ is $45°$ (see the plots with $\theta = 45°$), while the amplitude of the resonance signal at $2\omega_0$ is independent of α only when both $\phi = 90°$ and $\theta = 45°$ are satisfied (see the $\phi = 90°, \theta = 45°$ plot).

The information carried by the two groups of magnetic resonances can be used to construct a dead-zone-free all-optical magnetometer. One can always obtain a nonzero resonance signal at $2\omega_0$ by adjusting the ellipticity of the light polarization in any magnetic-field direction. The theoretical simulation results are shown in Fig. 5(a). The minimum occurs

when $\phi = 90°$ and $\theta = 45°$. The ratio of the minimum to the maximum contrast is 25% theoretically. The signal amplitudes of the resonance at $2\omega_0$ produced by circularly [Fig. 5(c)] or linearly [Fig. 5(e)] polarized light are also presented for comparison. An electro-optic modulator [21] or a Mach-Zehnder interferometer [38] could be used to control the ellipticity of the light polarization. Adding a slight low-frequency modulation to the ellipticity, which would cause a modulation of the signal amplitude, and the demodulated signal could be used as an error signal to automatically control the ellipticity of the light polarization. Other parameters influencing the signal amplitude should be properly handled. For instance, the laser frequency and intensity stabilization systems are needed to reduce the fluctuations of the laser frequency and intensity. In addition, utilizing both resonances at ω_0 and $2\omega_0$, along with adjusting the ellipticity of the light polarization, amplitude losses due to the magnetic-field direction could be notably
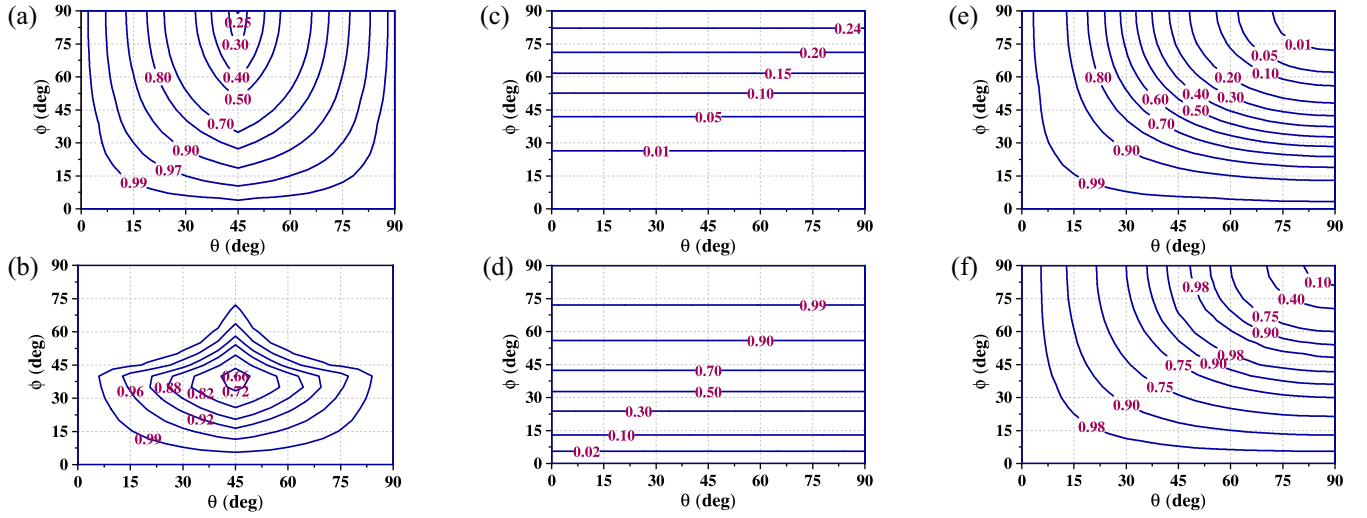
FIG. 5. The six contour plots based on the theoretical simulation results from Eqs. (A3) show the dependence of the resonance signal amplitudes on magnetic-field direction. The amplitudes of resonance signals are represented in percent of the maximum amplitude. (a) and (b) Ellipticity of the light polarization is adjusted to obtain the maximum amplitude of the resonance signal in each magnetic-field direction. (c) and (d) Circularly polarized light $\alpha = 45°$. (e) and (f) Linearly polarized light $\alpha = 0°$. (a) Only resonances at $2\omega_0$ are used. The minimum signal amplitude is 25% of the maximum. (b) Both resonances at ω_0 and $2\omega_0$ are used. The minimum signal amplitude is 64% of the maximum. (c) Only resonances at $2\omega_0$ are utilized and $\phi = 0°$ are dead zones. (d) Both resonances at ω_0 and $2\omega_0$ are utilized and $\phi = 0°$ are dead zones. (e) Only resonances at $2\omega_0$ are employed. Dead zones appear when both ϕ and θ equal $90°$. (f) Both resonances at ω_0 and $2\omega_0$ are employed. Dead zones occur when both ϕ and θ equal $90°$.

reduced. The theoretical simulation results are shown in Fig. 5(b). The ratio of the minimum to the maximum contrast is 64% theoretically and 62% experimentally. The maximal amplitudes of the two resonances at ω_0 and at $2\omega_0$ induced with circularly [Fig. 5(d)] or linearly [Fig. 5(f)] polarized light are also presented for comparison. Since the linewidth of the signal is independent of the magnetic-field direction, the sensitivity losses due to the magnetic-field direction can also be strongly suppressed.

Another effect related to the direction of the magnetic field is the heading error, which is mainly caused by the vector light shift (VLS) in ^{4}He magnetometers. The VLS is equivalent to a virtual magnetic field when the light is off-resonance. When the magnitude of the external magnetic field is much larger than that of the virtual magnetic field caused by the VLS, only the projection of the virtual magnetic field on the magnetic-field direction needs to be taken into account [39]. From Eqs. (A1) and (10) we know that the virtual magnetic field along the direction of the magnetic field can be written as

$$\delta B_z = \frac{E_0^2 D_0^2 \Delta}{3\gamma \left(\Delta^2 + \Gamma_e^2 \right)} \sin 2\epsilon \cos \phi. \quad (26)$$

In this study, the VLS could be neglected because the laser frequency could be tuned resonantly with the ^{4}He D_0 transition line, i.e., $\Delta = 0$.

V. CONCLUSION

In this paper, in the low-light-power limit, we studied the magneto-optical resonance spectra of the metastable ^{4}He atoms with intensity-modulated arbitrarily polarized resonant light in the presence of a quasistatic magnetic field of arbitrary direction. We present analytical expressions for the absorption signals and observe two independent groups of magnetic resonance signals at the Larmor frequency ω_0 and at its second harmonic $2\omega_0$. The linewidth and phase of the resonance signals at ω_0 and at $2\omega_0$ are both independent of the magnetic-field direction and the ellipticity of the light polarization. However, the amplitudes of the resonance signals at ω_0 and at $2\omega_0$ have a strong dependence on the ellipticity of the light polarization and the magnetic-field direction. Experimental results show agreement with theoretical predictions. In addition, utilizing both resonances at ω_0 and at $2\omega_0$, the amplitude and sensitivity losses due to the magnetic-field direction could be strongly suppressed by adjusting the ellipticity of the light polarization. This conclusion makes our results practical for future application to all-optical atomic magnetometers without dead zones. Furthermore, the orientational dependence of the signal amplitude on the external magnetic-field direction may be helpful when realizing a vector magnetometer.

APPENDIX: LONG EXPRESSIONS

This Appendix shows the long expressions in Sec. III. The components of Φ are

$$\langle \mathsf{J}_z \rangle_L = \mathrm{Tr}[\Phi \mathsf{J}_z] = \sin 2\epsilon \cos \phi, \tag{A1a}$$

$$\langle \mathsf{J}_+ \rangle_L = \mathrm{Tr}[\Phi \mathsf{J}_+] = -i \sin 2\epsilon \sin \phi, \tag{A1b}$$

$$\left\langle \mathsf{T}_2^{(2)} \right\rangle_L = \mathrm{Tr}\left[\Phi \mathsf{T}_2^{(2)}\right] = \frac{1}{2}[\sin^2 \epsilon (\cos \theta \cos \phi + i \sin \theta)^2 - \cos^2 \epsilon (\cos \theta + i \sin \theta \cos \phi)^2], \tag{A1c}$$

$$\left\langle \mathsf{T}_1^{(2)} \right\rangle_L = \mathrm{Tr}\left[\Phi \mathsf{T}_1^{(2)}\right] = i \sin \phi (\cos^2 \theta \sin^2 \epsilon \cos \phi + \sin^2 \theta \cos^2 \epsilon \cos \phi - i \sin \theta \cos \theta \cos 2\epsilon), \tag{A1d}$$

$$\left\langle \mathsf{T}_0^{(2)} \right\rangle_L = \mathrm{Tr}\left[\Phi \mathsf{T}_0^{(2)}\right] = \frac{1}{4\sqrt{6}}(1 + 3\cos 2\phi + 6\cos 2\theta \cos 2\epsilon \sin^2 \phi), \tag{A1e}$$

$$\langle \mathsf{J}_- \rangle_L = \langle \mathsf{J}_+ \rangle_L^*, \quad \left\langle \mathsf{T}_{-1}^{(2)} \right\rangle_L = -\left\langle \mathsf{T}_1^{(2)} \right\rangle_L^*, \quad \left\langle \mathsf{T}_{-2}^{(2)} \right\rangle_L = \left\langle \mathsf{T}_2^{(2)} \right\rangle_L^*. \tag{A1f}$$

The steady-state solution of Eq. (19) is

$$\langle \mathsf{J}_z \rangle = \frac{\gamma_p \sin 2\epsilon \cos \phi [\Gamma^2 + \Gamma \Omega (\Gamma \cos \omega t + \omega \sin \omega t) + \omega^2]}{\Gamma(\Gamma^2 + \omega^2)}, \tag{A2a}$$

$$\langle \mathsf{J}_+ \rangle = -\frac{i\gamma_p \sin 2\epsilon \sin \phi \{(\Gamma + i\omega_0)^2 + \Omega(\Gamma + i\omega_0)[\omega \sin \omega t + (\Gamma + i\omega_0)\cos \omega t] + \omega^2\}}{(\Gamma + i\omega_0)[\omega^2 + (\Gamma + i\omega_0)^2]}, \tag{A2b}$$

$$\left\langle \mathsf{T}_2^{(2)} \right\rangle = -\frac{\gamma_p[\cos 2\epsilon (\cos 2\theta \cos 2\phi + 4i \sin 2\theta \cos \phi) + 3\cos 2\epsilon \cos 2\theta + 2\sin^2 \phi]}{8(\Gamma + 2i\omega_0)[\omega^2 + (\Gamma + 2i\omega_0)^2]}$$
$$\times \{(\Gamma + 2i\omega_0)^2 + \Omega(\Gamma + 2i\omega_0)[\omega \sin \omega t + (\Gamma + 2i\omega_0)\cos \omega t] + \omega^2\}, \tag{A2c}$$

$$\left\langle \mathsf{T}_1^{(2)} \right\rangle = \frac{\gamma_p \sin \phi [\sin 2\theta \cos 2\epsilon + i \cos \phi (1 - \cos 2\theta \cos 2\epsilon)]\{(\Gamma + i\omega_0)^2 + \Omega(\Gamma + i\omega_0)[\omega \sin \omega t + (\Gamma + i\omega_0)\cos \omega t] + \omega^2\}}{2(\Gamma + i\omega_0)[\omega^2 + (\Gamma + i\omega_0)^2]}, \tag{A2d}$$

$$\left\langle \mathsf{T}_0^{(2)} \right\rangle = \frac{\gamma_p (1 + 3\cos 2\phi + 6\cos 2\theta \cos 2\epsilon \sin^2 \phi)[\Gamma^2 + \Gamma \Omega (\Gamma \cos \omega t + \omega \sin \omega t) + \omega^2]}{4\sqrt{6}\Gamma(\Gamma^2 + \omega^2)}, \tag{A2e}$$

$$\langle \mathsf{J}_- \rangle = \langle \mathsf{J}_+ \rangle^*, \quad \left\langle \mathsf{T}_{-1}^{(2)} \right\rangle = -\left\langle \mathsf{T}_1^{(2)} \right\rangle^*, \quad \left\langle \mathsf{T}_{-2}^{(2)} \right\rangle = \left\langle \mathsf{T}_2^{(2)} \right\rangle^*. \tag{A2f}$$

The functions $f_1(\theta, \phi, \epsilon)$ and $f_2(\theta, \phi, \epsilon)$ are

$$f_1(\theta, \phi, \epsilon) = \tfrac{1}{4} \sin^2 \phi (1 - \cos 2\theta \cos 2\epsilon)(1 + \cos^2 \phi + \cos 2\theta \cos 2\epsilon \sin^2 \phi), \tag{A3a}$$

$$f_2(\theta, \phi, \epsilon) = \tfrac{1}{512}\{3\cos 4\theta + 4\cos 4\phi (1 - \cos 2\theta \cos 2\epsilon)^2 + 4\cos 2\phi [3 + 7\cos 4\epsilon - 2\cos 2\epsilon (4\cos 2\theta + \cos 4\theta \cos 2\epsilon)]$$
$$+ 40\cos 2\theta \cos 2\epsilon + 3\cos 4\theta \cos 4\epsilon + 35\cos 4\epsilon + 47\}. \tag{A3b}$$

[1] I. Kominis, T. Kornack, J. Allred, and M. V. Romalis, Nature (London) **422**, 596 (2003).

[2] D. Budker and M. Romalis, Nat. Phys. **3**, 227 (2007).

[3] E. Boto, N. Holmes, J. Leggett, G. Roberts, V. Shah, S. S. Meyer, L. D. Muñoz, K. J. Mullinger, T. M. Tierney, S. Bestmann, G. R. Barnes, R. Bowtell, and M. J. Brookes, Nature (London) **555**, 657 (2018).

[4] S. Colombo, V. Lebedev, A. Tonyushkin, S. Pengue, and A. Weis, IEEE Trans. Med. Imaging **39**, 922 (2020).

[5] N. Olsen, G. Hulot, V. Lesur, C. C. Finlay, C. Beggan, A. Chulliat, T. J. Sabaka, R. Floberghagen, E. Friis-Christensen, and R. Haagmans, Geophys. Res. Lett. **42**, 1092 (2015).

[6] A. Balogh, Space Sci. Rev. **152**, 23 (2010).

[7] J. W. Blanchard, T. Wu, J. Eills, Y. Hu, and D. Budker, J. Magn. Reson. **314**, 106723 (2020).

[8] M. S. Safronova, D. Budker, D. DeMille, D. F. Jackson Kimball, A. Derevianko, and C. W. Clark, Rev. Mod. Phys. **90**, 025008 (2018).

[9] D. Budker and D. F. J. Kimball, *Optical Magnetometry* (Cambridge University Press, Cambridge, 2013).

[10] A. Weis, G. Bison, and A. S. Pazgalev, Phys. Rev. A **74**, 033401 (2006).

[11] A. Weis, G. Bison, and Z. D. Grujić, in *High Sensitivity Magnetometers*, edited by A. Grosz, M. J. Haji-Sheikh, and S. C. Mukhopadhyay (Springer, Cham, 2017), pp. 361–424.

[12] S. Colombo, V. Dolgovskiy, T. Scholtes, Z. D. Grujić, V. Lebedev, and A. Weis, Appl. Phys. B **123**, 35 (2017).

[13] S. J. Ingleby, C. O'Dwyer, P. F. Griffin, A. S. Arnold, and E. Riis, Phys. Rev. A **96**, 013429 (2017).

[14] M. K. Plante, D. L. MacFarlane, D. D. McGregor, R. E. Slocum, W. M. Sampson, and A. W. Brown, Phys. Rev. A **82**, 013837 (2010).

[15] M. K. Plante, A generalized theory of double-resonance laser-pumped helium-4 magnetometers, Ph.D. thesis, The University of Texas at Dallas, 2010.

[16] W. E. Bell and A. L. Bloom, Phys. Rev. Lett. **6**, 280 (1961).

[17] W. E. Bell and A. L. Bloom, Phys. Rev. Lett. **6**, 623 (1961).

[18] D. Budker, W. Gawlik, D. F. Kimball, S. M. Rochester, V. V. Yashchuk, and A. Weis, Rev. Mod. Phys. **74**, 1153 (2002).

[19] D. Budker, D. F. Kimball, V. V. Yashchuk, and M. Zolotorev, Phys. Rev. A **65**, 055403 (2002).

[20] V. Schultze, R. IJsselsteijn, T. Scholtes, S. Woetzel, and H.-G. Meyer, Opt. Express **20**, 14201 (2012).

[21] A. Ben-Kish and M. V. Romalis, Phys. Rev. Lett. **105**, 193601 (2010).

[22] G. Bevilacqua and E. Breschi, Phys. Rev. A **89**, 062507 (2014).

[23] A. Cassimi, B. Chéron, and J. Hamel, J. Phys. II (France) **1**, 123 (1991).

[24] B. Chéron, H. Gilles, J. Hamel, O. Moreau, and E. Noël, J. Phys. II (France) **6**, 175 (1996).

[25] C. Guttin, J. Léger, and F. Stoeckel, J. Phys. IV (France) **4**, C4-655 (1994).

[26] J. Rutkowski, W. Fourcault, F. Bertrand, U. Rossini, S. Gétin, S. Le Calvez, T. Jager, E. Herth, C. Gorecki, M. Le Prado *et al.*, Sens. Actuat. A **216**, 386 (2014).

[27] B. Chéron, H. Gilles, J. Hamel, O. Moreau, and E. Noël, J. Phys. III (France) **7**, 1735 (1997).

[28] B. Chéron, H. Gilles, and J. Hamel, Eur. Phys. J. Appl. Phys. **13**, 143 (2001).

[29] G. Lieb, T. Jager, A. Palacios-Laloy, and H. Gilles, Rev. Sci. Instrum. **90**, 075104 (2019).

[30] T. Wu, X. Peng, Z. Lin, and H. Guo, Rev. Sci. Instrum. **86**, 103105 (2015).

[31] Z. D. Grujić and A. Weis, Phys. Rev. A **88**, 012508 (2013).

[32] T. Wu, X. Peng, W. Gong, Y. Zhan, Z. Lin, B. Luo, and H. Guo, Opt. Lett. **38**, 986 (2013).

[33] W. Happer, Rev. Mod. Phys. **44**, 169 (1972).

[34] G. Bevilacqua, E. Breschi, and A. Weis, Phys. Rev. A **89**, 033406 (2014).

[35] D. D. McGregor, Rev. Sci. Instrum. **58**, 1067 (1987).

[36] E. Breschi, Z. D. Grujić, P. Knowles, and A. Weis, Phys. Rev. A **88**, 022506 (2013).

[37] D. F. Jackson Kimball, J. Dudley, Y. Li, and D. Patel, Phys. Rev. A **96**, 033823 (2017).

[38] P. Włodarczyk, S. Pustelny, and D. Budker, Rev. Sci. Instrum. **90**, 013110 (2019).

[39] G. Oelsner, V. Schultze, R. IJsselsteijn, F. Wittkämper, and R. Stolz, Phys. Rev. A **99**, 013420 (2019).